# PICOSEC Micromegas gaseous detectors for precise timing and developments towards applicable detector

Francesco Guerra[1,2], Marta Lisowska[2], Eraldo Oliveri[2] and Florian Brunbauer[2]

[1] Physics Department, University of Turin
[2] European Organization for Nuclear Research (CERN)

## Abstract :

The PICOSEC Micromegas project aims to develop a scalable gaseous detector capable of achieving time resolutions of O(10) ps for future high-energy physics experiments.
In this work, signal analysis techniques and results from beam tests of different PICOSEC prototypes, including single-channel devices with various photocathode materials (CsI, Ti, and $B_4C$) and a 100-channel prototype based on a novel double-layer DLC resistive Micromegas design are presented.
Test beam results demonstrate that thinner photocathodes systematically improve time resolution, with titanium emerging as a promising compromise between performance and robustness. For the multi-pad prototype, a reconstruction algorithm based on amplitude-weighted averaging yielded spatial resolutions of 2.9 mm (x) and 2.5 mm (y) over 10 mm x 10 mm pads, while different strategies for combining timing information across pads were compared. Comparable results were obtained using a time-resolution-weighted and a charge-weighted approach.
These studies confirm the potential of PICOSEC Micromegas detectors to combine excellent timing, robustness, and scalability, thereby paving the way toward their application in future high-energy physics experiments.

**Keywords:** PICOSEC, Micromegas, Timing detectors, Photocathodes, Gaseous detectors

## 1 Introduction

Future high energy physics experiments will require precise time, energy and position measurements, demanding a new generation of particle detectors with increasing accuracy. In particular, time resolutions of the order of O(30) ps are required to mitigate pileup-induced background for the high-luminosity era of LHC and to enhance particle identification through Time-of-Flight (ToF) measurements [1].
The ATLAS and CMS upgrades foreseen for HL-LHC are focused on silicon-based detectors to achieve the required timing capabilities; nonetheless the harsh irradiation conditions and the considerable costs restrict these technologies to applications of few square meters. To cover large areas while maintaining excellent spatial resolution, high-rate resistance and relatively low costs, Micro-Pattern Gaseous Detectors (MPGDs) are natural candidates to be investigated [2].
The PICOSEC Micromegas project is developing a spatially scalable, stable and robust gaseous detector with time resolution of the order of O(10) ps. Through successive phases of development, intensive research to enhance the detector ultimately achieved a time resolution of 12.5 ps [3].

### 1.1 Detector concept

The PICOSEC detector consists of a two-stage Micromegas (MM) amplification structure [4] with a semi-transparent photocathode coupled to a Cherenkov radiator. The main idea behind this novel gaseous detector design is to suppress the time jitter coming from different ionization cluster position in a standard MM. The passage of a charged particle through the radiator produces UV photons by Cherenkov effect; these photons interact with the photocathode leading to the emission of photoelectrons, which are then amplified by the Micromegas structure [5]. This mechanism allows to overcome the standard MM limitation, enabling the creation of primary electrons synchronously and at the same distance from the mesh. Furthermore, in order to minimize the longitudinal diffusion and the probability of direct ionization, the drift gap thickness is reduced at the level of 100-200 $\mu$m and employed as a pre-amplification stage.
The detector is typically a bulk Micromegas filled with the *COMPASS* gas mixture ($Ne:C_2H_6:CF_4$ - 80:10:10) [6] at ambient pressure and uses a 3 mm thick $MgF_2$ crystal as radiator with the photocathode coated directly on it.

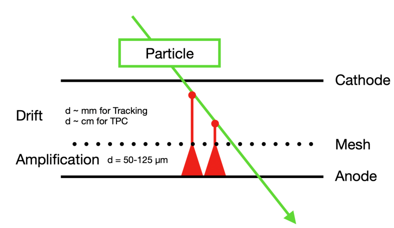


**Figure 1.** Standard Micromegas schematic [7]

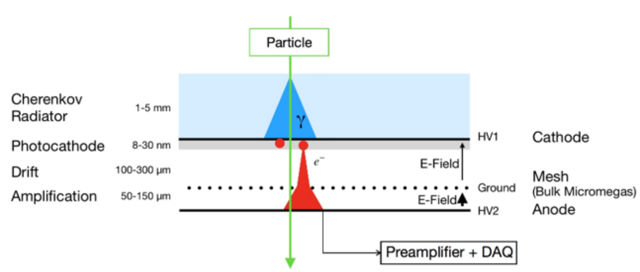


**Figure 2.** PICOSEC Micromegas schematic [5]

### *1.2 Developments towards applicable detector*

Currently, several efforts are underway to make the detector applicable in practice, with different prototypes being tested for this purpose.
The single-channel prototype (ø 10 or 15 mm) [3] features an optimized design aimed at exploiting the full potential of this technology and is primarily used to optimise detector parameters such as the resistivity of the anode layer[1], the thickness of the pre-amplification gap and, most importantly, the choice of photocathode material.

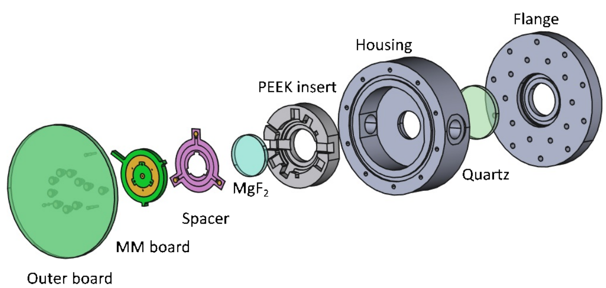


**Figure 3.** Exploded view of the single channel prototype [3]

The selection of the photocathode is crucial, as higher quantum efficiency - resulting in a greater number of emitted photoelectrons — helps to compensate for the statistical fluctuations arising from the amplification process [8]. At present, CsI provides the best performance due to its high quantum efficiency in semi-transparent mode; however, aging studies indicate that it rapidly deteriorates after irradiation and is highly sensitive to humidity. Consequently, one of the main concerns of the PICOSEC collaboration is identifying robust alternatives to CsI that can maintain excellent time resolution while ensuring long-term stability. To this end, materials such as Ti, diamond-like carbon (DLC) and $B_4C$ with different thicknesses are currently under investigation [9, 10]. In addition, in order to increase both the area coverage and the spatial resolution of the detector, different multi-pad prototypes are currently under evaluation [11, 12]. These include the so-called high- and medium-granularity designs, which employ small hexagonal pads, as well as a 100-channel prototype featuring square pads of 10 mm × 10 mm. Alongside these developments, novel approaches such as double resistive layer DLC structures and scalable electronics are also being investigated.
Equally important are the studies on alternative gas mixtures that could replace $CF_4$, which is currently used but has a high global warming potential. A potential issue is that, in the near future, purchasing this gas may become either impossible or prohibitively expensive due to regulatory restrictions. In this context, mixtures based on noble gases combined with isobutane are currently being investigated.

## 2 Signal analysis

A representative signal from the PICOSEC-MM is shown in Fig. 4. It consists of a fast electron peak, generated by the rapid multiplication and movement of electrons towards the anode, followed by a slower ion tail produced by the ions moving in the opposite direction towards the mesh.

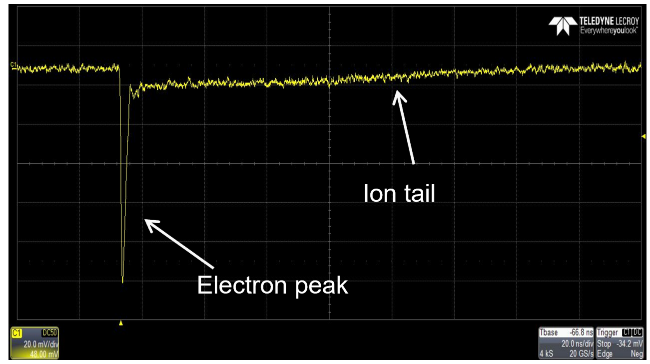


**Figure 4.** PICOSEC signal seen at the oscilloscope using a RF current preamplifier.

For timing purposes, the relevant information is carried by the leading edge of the electron peak, which exhibits a rise time of less than 1 ns. To preserve this timing information, the signals are typically amplified using RF amplifiers (based on [13]) and read out with oscilloscopes or dedicated digitizers (e.g. SAMPIC [14]). The recorded waveforms are subsequently analyzed offline to evaluate the detector performance. The standard analysis procedure is as follows [10]: (i) the baseline offset and noise level are determined from the pre-trigger region; (ii) the maximum amplitude, $V_{max}$, is obtained after baseline subtraction; (iii) the start and end points of the signal are defined as the first and last samples around the peak deviating from the baseline by more than one noise RMS; (iv) the electron peak charge is calculated by integrating the waveform between these two points and converting the result to pC using the 50 Ω input impedance; and (v) the leading edge of the electron peak is fitted with a sigmoid function, from which the rise time is extracted and a timestamp is defined using constant fraction discrimination (CFD) at 20% of the signal amplitude. When a time reference signal is available, the same processing is applied to it, and the Signal Arrival Time (SAT) is defined as the difference between the reference timestamp and that of the device under test (DUT). After applying a possible time-walk correction to the SAT, the spread of the SAT distribution provides a measurement of the DUT time resolution.

### *2.1 Single photoelectron measurements*

In general, when operating a gaseous detector, it is essential to verify that the obtained results are reproducible. Since the detector response depends on several parameters, one method to characterize the device (e.g., gain, rise time) and to ensure consistency throughout the data-taking campaign is to perform single-photoelectron (SPE) measurements [15]. Moreover, because the number of photoelectrons emitted by the photocathode is a dominant factor in determining the time resolution, the average number of photoelectrons per particle passage can be estimated by comparing the mean signal amplitude from a traversing particle with that from single-photoelectron events.
For this purpose, the detector can be illuminated with UV light from a LED operated at very low intensity, such that the resulting signals predominantly correspond to the emission of a single pho-

[1] The resistive anode enables operation at slightly higher gain providing protection against discharges.

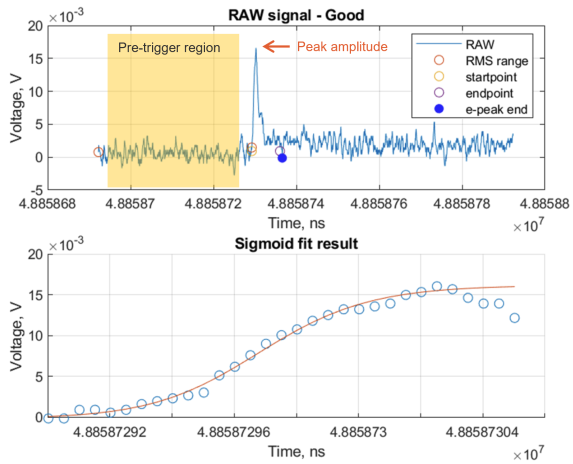


**Figure 5.** General waveform analysis.

toelectron per event. By acquiring these waveforms and analyzing the distribution of their amplitudes (or integrated charge), the avalanche dynamics inside the detector can be studied and modeled through a Polya distribution.

In this configuration, the waveforms are acquired without an external trigger and without timing information, making the optimization of the signal-to-noise ratio (SNR) particularly critical. A high trigger threshold suppresses noise but introduces bias by excluding low-amplitude events, while a low threshold leads to noise-dominated distributions (Fig. 6).

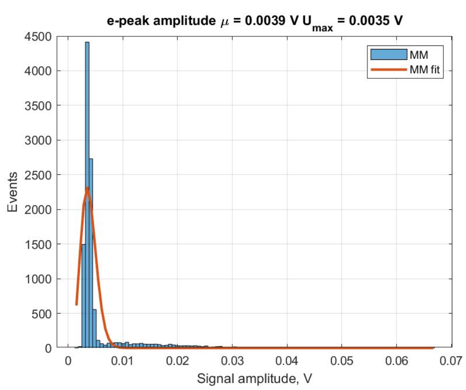


**Figure 6.** Example of noise dominated distribution

Historically, dedicated slow preamplifiers with superior SNR have been employed for SPE measurements; however, these cannot be used for precise timing, which requires fast amplifiers. The use of the fast amplifier offers an additional advantage: beyond avoiding the need to continuously switch amplifiers during data taking, the recorded waveforms make it possible to identify specific types of events, such as multi-peak signals, likely caused by photon feedback. The adopted strategy consisted in applying a relatively low trigger threshold on the oscilloscope — thus acquiring both signal and noise — and subsequently rejecting noise offline.

To enhance noise rejection, the recorded signals were processed using a Savitzky–Golay smoothing filter [16], which preserves the peak structure while reducing high-frequency fluctuations. This "simplified" version of the waveform enabled the reliable extraction of basic signal features. In particular, it allowed: (i) improved determination of the electron peak end (defined as the intersection of two linear fits applied to the falling edge of the electron peak and to the flat ion-tail region); (ii) definition of the ion-tail end as the last point exceeding the RMS noise of the smoothed waveform; (iii) identification of multiple peaks, likely due to photon feedback, by analyzing local maxima and their separation; and (iv) rejection of noise events in which the maximum amplitude of the smoothed waveform — corresponding to the electron peak — was less than three times the baseline noise RMS above the ion-tail average value.

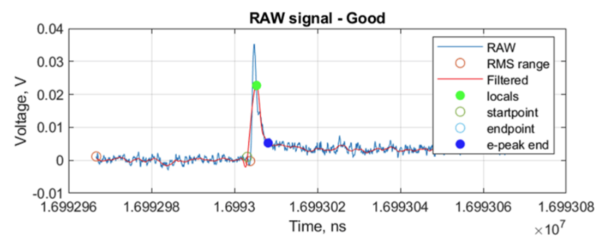


**Figure 7.** Smoothed waveform analysis

Thanks to this noise-rejection strategy and to the improved identification of the ion-tail end, it was possible to obtain amplitude and charge distributions less affected by low-amplitude noise. By integrating the waveform from the start point to the ion-tail end — emulating the response of a charge-sensitive amplifier — distributions with a clearer separation between noise and true SPE signals were achieved.

The algorithm was tested using a titanium photocathode, which can be operated at high gain even under beam conditions due to the low number of photoelectrons produced, and the parameters were optimized for this case. However, for photocathodes with a higher QE operated at lower gain such as CsI, the amount of noise picked up in SPE measurements proved too large to be effectively handled with this approach.

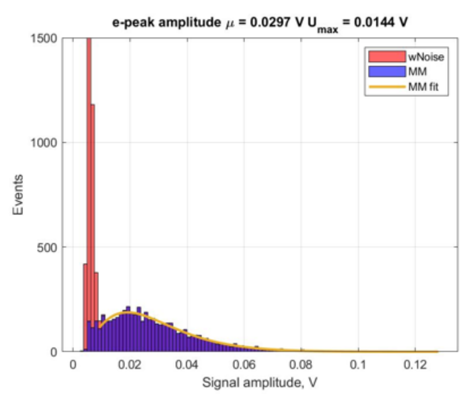


**Figure 8.** Example of amplitude spectrum obtained with SPE measurements - in red with the standard analysis and in blue with the smoothed one

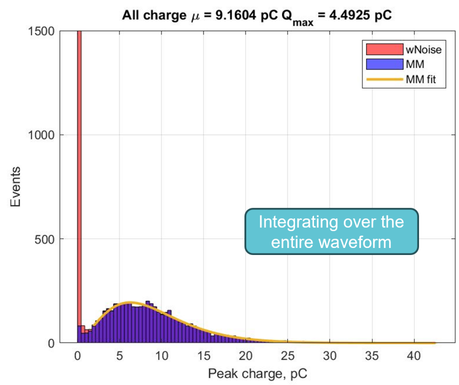


**Figure 9.** Example of charge spectrum obtained with SPE measurements - in red recognized noise events and in blue signal events

**Future prospects:** Future improvements of the algorithm may include parameter tuning for low-gain operation or the application of machine-learning techniques for noise rejection. Nevertheless, the intrinsic bias introduced by triggering on the signal itself remains an open issue and warrants further investigation.
Regarding the measurements themselves, given their importance in characterizing the detector response, several aspects still require clarification. First, as also noted in previous work [17], it has been observed that using the same detector with different photocathodes or housings can yield different results under identical field settings, for reasons that are not yet understood. This calls for systematic studies to identify the factors that may play a role. Moreover, in order to assess the reproducibility of the results and to verify whether the experimental conditions change during data taking (e.g. for sealed mode operation), SPE measurements should be performed both before and after each particle-beam run. This approach could also be beneficial in the case of CsI: although it is not possible to perform measurements at the exact operating point used under beam conditions, acquiring SPE spectra at higher gain would still provide valuable information.

## 3 Test beam measurements

To evaluate the performance of the PICOSEC prototypes with charged particles, test beam facilities at CERN were utilized. Within the framework of a test beam campaign organized by the DRD1 collaboration, prototypes were exposed to a muon beam at the CERN SPS H4 beam line. During this campaign, different prototypes and several aspects of the detector performance were investigated. In particular, my work focused on single-channel prototypes equipped with photocathodes of varying thicknesses (CsI, Ti, and $B_4C$), as well as on a 100-channel prototype featuring double DLC resistive layers for vertical charge evacuation combined with a Ti photocathode.

### *3.1 Setup*

To investigate the performance of the PICOSEC-MM under particle beam conditions, it is essential to employ detectors that provide a trigger for the data acquisition system (DAQ), serve as a precise time reference (for assessing the time resolution), and deliver information on the particle trajectory through the device under test (DUT), which in turn defines the region where the Cherenkov cone is distributed across the active area. For this purpose, the PICOSEC collaboration employs the telescope setup shown in Fig. 10 [11]. The telescope consists of three triple-GEM detectors, read out by APV25 chips and the Scalable Readout system (SRS) [18, 19] to provide tracking information, together with a micro-channel plate photomultiplier tube (MCP-PMT) mounted on a movable stage. The MCP-PMT is used both as the trigger and as the time reference, owing to its excellent timing performance, with a resolution of approximately 6 ps in the central region[2] [15]. In this context, tracking information is of fundamental importance: it allows the selection of tracks passing through the optimal region of the MCP, ensures proper alignment between the MCP and the DUT and enables the characterization of events occurring in the detector's active area (e.g., in multi-pad prototypes) by exploiting geometrical information.

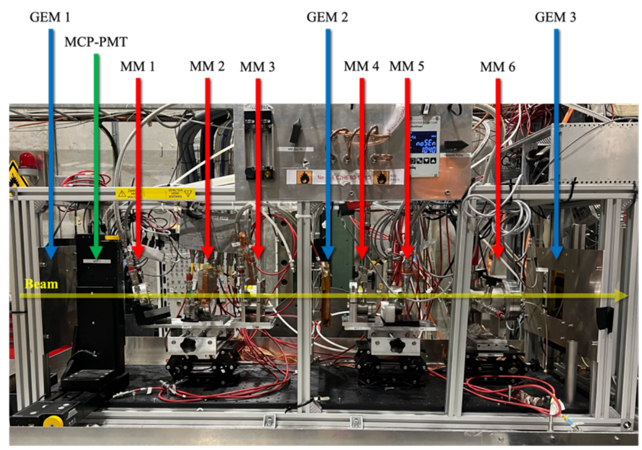


**Figure 10.** PICOSEC telescope [10]

Once data are acquired with both the additional time reference and tracking information, the subsequent signal processing and analysis follow the methodology described in Section 2. In particular, the amplitude variation over the detector surface is employed to determine the center of the active area. Knowing the DUT center allows one to define a region of interest corresponding to events in which the Cherenkov cone is fully contained within the active area. Finally, after applying a time-walk correction based on the correlation between the Signal Arrival Time (SAT) and the electron-peak charge, the time resolution is extracted from the SAT distribution by means of a double-Gaussian fit.

### *3.2 Photocathode studies*

As mentioned earlier in this report, the number of primary electrons emitted by the photocathode plays a key role in determining the achievable time resolution ($\sigma \propto 1/\sqrt{N_{PE}}$).
When photocathodes are operated in semi-transparent mode, photons produced in the radiator must interact with the photocathode material, while the resulting photoelectrons need to be emitted from the opposite side in order to enter the gas region. This introduces a trade-off between the probability of photon interaction

[2] Time resolution of the MCP was estimated doing a run using two identical MCPs (one as reference, one as device under test) during this test beam campaign

and photoelectron emission, and the probability of photoelectrons being extracted into the gas. For this reason, particularly when exploring new materials, it is essential to scan different photocathode thicknesses to determine the optimal configuration, also taking into account the limitations imposed by production techniques.
In addition to robust options such as Ti and $B_4C$, CsI photocathodes were also tested. Previously, the optimal thickness for CsI had been identified as 18 nm; however, building on the knowledge acquired over the years and the improved time resolution achieved, other thicknesses were also investigated.
For each photocathode, a voltage scan was performed to determine the optimal operating point. The voltages were scanned primarily at the photocathode level, taking into account the maximum charge the detector could safely withstand. Since the number of primary electrons emitted differs between photocathodes, the applied voltages were adjusted accordingly.
The resulting plots, showing the RMS of the SAT distribution as a function of the average amplitude, are reported below.

| Material | Thickness (nm) | Cath./Anode (V) | $RMS_{SAT}$ (ps) |
|---|---|---|---|
| CsI | 3 | -440/275 | 11.4 |
| Ti | 2.5 | -490/275 | 31.5 |
| $B_4C$ | 5 | -490/275 | 43 |

**Table 1**
Best performance for each photocathode material

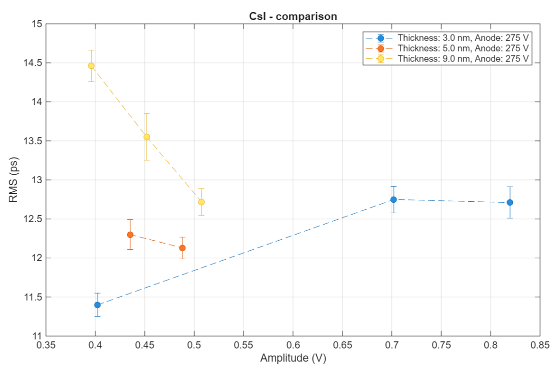


**Figure 11.** Time resolution for different CsI thicknesses

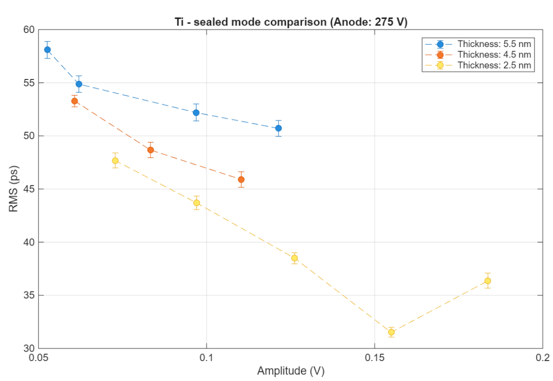


**Figure 12.** Time resolution for different Ti thicknesses

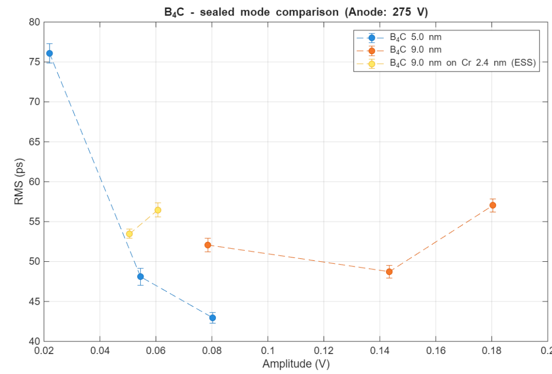


**Figure 13.** Time resolution for different $B_4C$ thicknesses

In most cases, the thinnest layers exhibited the best performance, which can be attributed to the fact that thinner films facilitate the extraction of photoelectrons while still providing sufficient material for photon interaction [10].
These results motivate further investigations into alternative materials such as titanium, which combine excellent time resolution with robustness and radiation hardness [20].

### 3.3 *Double layer DLC resistive Micromegas*

To explore a solution with potential for practical applicability, a double-layer DLC resistive Micromegas equipped with a 2.4 nm Ti photocathode was tested. Over the past decade, the use of resistive anodes in gaseous detectors has been extensively investigated as a means of improving protection against discharge phenomena. One of the main limitations of this approach are the accumulation of induced charge on the resistive layer, which is only slowly evacuated through the bias points of the layer - thereby limiting the detector's rate capability, and the voltage drop caused by the moving charges in a resistive medium that changes the electric field. The double-resistive-layer concept addresses this limitations by interconnecting the two layers to the readout pads via vertical vias, thus enabling the charge collected on the first resistive layer to be evacuated vertically. This configuration enhances the rate capability while maintaining sufficient resistance to ensure discharge protection.

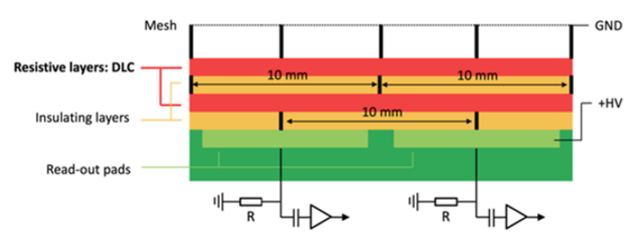


**Figure 14.** Double layer DLC concept [10]

The primary challenge in using a multi-pad detector is to preserve the time resolution when the Cherenkov cone is not fully contained within a single pad but instead distributed across multiple pads, producing several smaller signals [21]. To investigate this issue, four pads were selected from the 100-pad detector powered with -550 V at the cathode and 275 V at the anode, and a dedicated scan was performed with the MCP in the corresponding area. The four pads were connected to the oscilloscopes, which simultaneously recorded the time reference signal, the signal from each pad and the event ID provided by the DAQ system. The analysis strategy consisted first of studying the pads individually, using the information from each oscilloscope channel separately, and subsequently combining the pad information through the event ID.

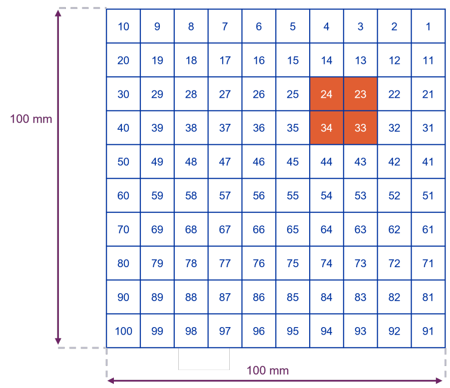


**Figure 15.** Pads selected on the multi-pad prototype to investigate sharing events

**3.3.1 Single pad analysis:** For the single-pad studies, the pad center was determined from the electron-peak charge distribution over the area, and cuts were applied on the SAT and rise-time distributions. This allowed the analysis to be performed in the same manner as for single-channel prototypes, using geometrical selections.

A critical aspect of this analysis concerns the choice and origin of the time-walk correction. When comparing the SAT correction applied to the central region of the pad with that applied to the full pad, a difference is observed (Figs. 16 - 19). As shown in [8], simulations of single-photoelectron events indicate that the dependence of SAT on the electron-peak charge arises from an intrinsic avalanche-time characteristic. However, this effect alone does not fully account for the observed discrepancies, and the underlying factors are still under investigation.

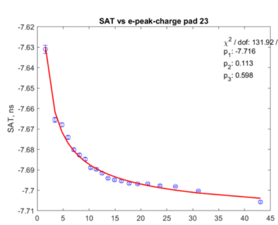


**Figure 16.** SAT vs e-peak charge - full pad

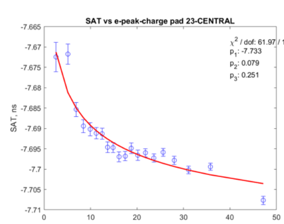


**Figure 17.** SAT vs e-peak charge - central part

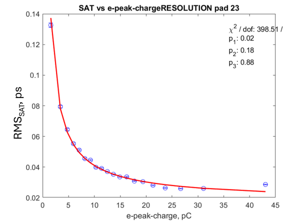


**Figure 18.** $RMS_{SAT}$ vs e-peak charge - full pad

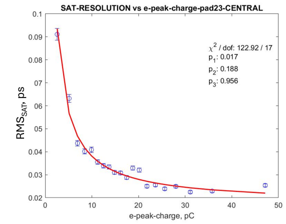


**Figure 19.** $RMS_{SAT}$ vs e-peak charge - central part

In addition, the algorithm used to extract the signal arrival time—namely the CFD applied to the leading edge of the electron-peak fitted with a sigmoid—may be influenced by variations in rise time or signal shape, which could reduce its effectiveness. This hypothesis is supported by the rise-time versus electron-peak charge plots (Figs. 20 and 21), where each pad exhibited a pattern similar to that observed for the SAT. Further studies are required to clarify the origin of this behavior and to assess whether an improved correction scheme can be developed that explicitly takes it into account.

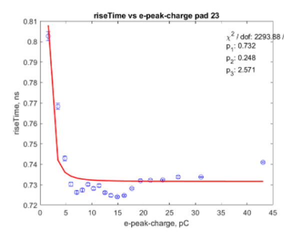


**Figure 20.** Rise time vs e-peak charge - full pad

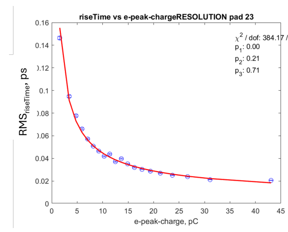


**Figure 21.** $RMS_{riseTime}$ vs e-peak charge - full pad

For the results presented in the following subsections, the SAT correction applied to each pad corresponds to that derived from the full-pad analysis.

| Pad | Avg. amplitude (V) | $RMS_{SAT}$ (ps) |
|---|---|---|
| 23 | 0.26 | 39 |
| 24 | 0.25 | 38 |
| 33 | 0.24 | 39 |
| 34 | 0.26 | 41 |

**Table 2**
Characterization for fully-contained events on each pad

Once the individual pad analysis was completed, the information on amplitude, electron-peak charge, SAT, and rise time was merged using the event ID, and for each event the active pads were identified. A detailed study was conducted to recognize the active pads and to rule out spurious signals correlated with the main ones.

**3.3.2 Observations on correlated spurious signals:** During the single-pad analysis, it was observed that the SAT distribution for the full set of events recorded on a given pad exhibited a double-peak structure (Fig. 22). However, when applying a geometrical selection restricted to the pad area, only a single peak was present. In addition, the correlation plot of SAT versus e-peak charge revealed that the events contributing to the “delayed” peak consistently corresponded to very low e-peak charges (Fig. 23).

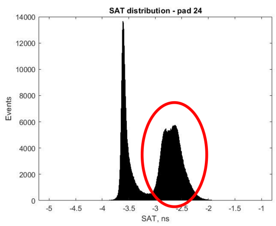


Figure 22. SAT distribution - full set of recorded events

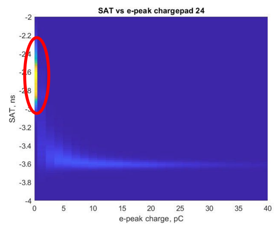


Figure 23. SAT vs e-peak charge correlation plot

Since such signals appeared only when the particle hit a different pad, a further study was performed by geometrically selecting events occurring at the center of another pad and analyzing the corresponding response on the pad under investigation. The results of this analysis are reported in Fig. 24, while an illustrative comparison between a spurious and a genuine signal is provided in Figs. 25 and 26.
As shown, for pad 23, when the geometrical selection was applied to an adjacent pad, the peak in the SAT distribution was delayed by approximately 700 ps, and the ratio between the real signal (in the geometrically selected pad) and the spurious one was about 17. In contrast, when the geometrical selection was applied to a diagonally opposite pad, the SAT delay increased to about 1 ns, and the ratio rose to approximately 23. The difference between the adjacent and diagonal cases suggests the appearance of a factor close to $\sqrt{2}$, which corresponds exactly to the ratio of the distances between pad centers in the two configurations. This observation indicates that the spurious signals might be the result of a propagation effect[3]. If this hypothesis is confirmed, time correlations could potentially be exploited to improve the position reconstruction on a pad, even in cases where the Cherenkov cone spreads only over a single pad. Further investigation is required to clarify the origin of this phenomenon and to assess its possible implications.

**3.3.3 Merged pad analysis:** By computing an amplitude-weighted average of the active pads, the particle impact position on the 10 mm × 10 mm pads was reconstructed. Comparison with the true impact position provided by the tracking system allowed the residuals (difference between reconstructed and true positions) to be evaluated, yielding spatial resolutions of 2.9 mm in the x-direction and 2.5 mm in the y-direction. A limiting factor in this reconstruction arises from the fact that the signal originates from photoelectrons produced by Cherenkov photons distributed over a cone of approximately 3 mm radius (given the 3 mm radiator thickness and a Cherenkov angle of ≈45°), which inherently degrades the achievable spatial resolution.

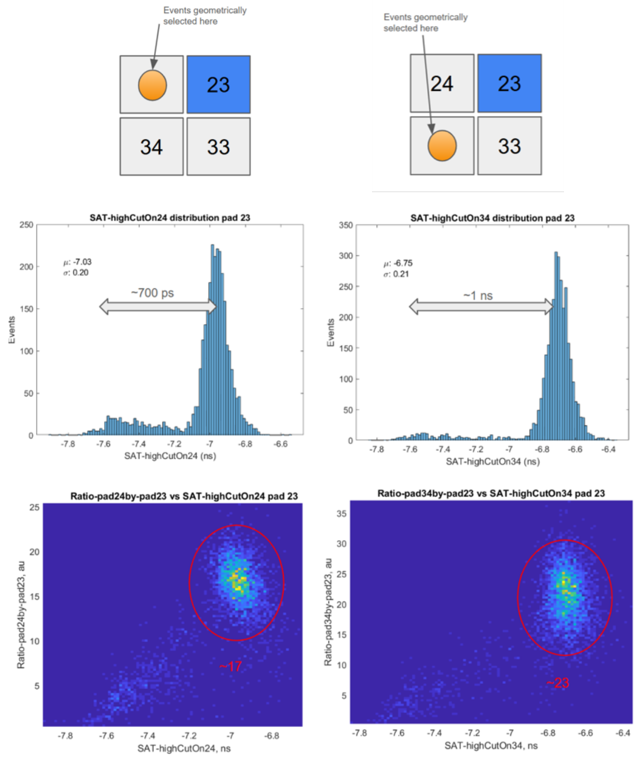


Figure 24. Pad 23 studies (adjacent and diagonal geometrical selections) - SAT distributions and correlations of SAT versus ratio of amplitudes between selected pad and pad 23 signals

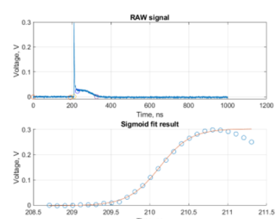


Figure 25. Real signal

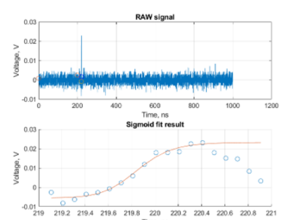


Figure 26. Spurious signal

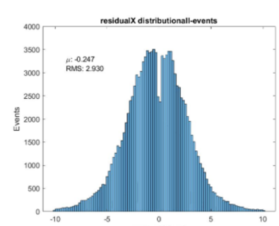


Figure 27. Residuals distribution - x direction

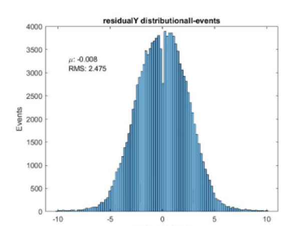


Figure 28. Residuals distribution - y direction

[3] The effect is probably not coming from the resistive layers because a similar phenomenon was observed analyzing data from a metallic multipad prototype tested in July 2022.

For the timing analysis, a single combined SAT was obtained by averaging the SAT values from all active pads, corrected for time-walk. Three weighting schemes were investigated: (i) using the parametrization of the time resolution versus electron-peak charge, with weights given by the inverse square of the time resolution; (ii) assigning weight 1 to the pad with the highest charge and 0 to the others; and (iii) using the electron-peak charge itself as the weight. A comparison of the results obtained with these three approaches is presented below.

| Method | $RMS_{SAT}$ (ps) |
|---|---|
| Time resolution | 45 |
| Highest charge | 48 |
| Electron-peak charge | 45 |

**Table 3**
Comparison of time resolution obtained in a 10 mm x 10 mm area between 4 pads using different combining methods

Comparable results were obtained using time resolution weighted and electron-peak charge weighted combining methods. Figs. 29 and 30 show the $RMS_{SAT}$ distribution across the area between the pads. It can be observed that the time resolution is not optimal over pads 23 and 33, which may be due either to less effective time-walk corrections applied in those regions or to other non-uniformities. A more detailed study is required to clarify this issue and to fully understand its origin.

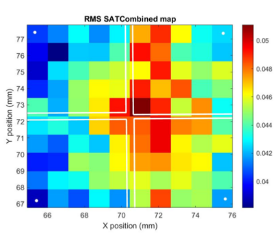


**Figure 29.** $RMS_{SAT}$ map between the pads

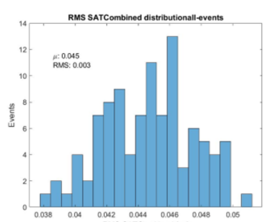


**Figure 30.** $RMS_{SAT}$ distribution in 1 mm x 1 mm squares over the selected area

**Future prospects:** Detailed studies are required to disentangle the various factors contributing to the observed SAT behavior. One possible approach, aimed at capturing the intrinsic avalanche-time characteristic even in shared events [8], would be to reconstruct the total avalanche charge for each event and then build the corresponding SAT calibration curve. In addition, investigating the role and origin of the rise-time variation with electron-peak charge could provide the basis for a more effective time-walk correction.
Another promising line of research concerns the correlated spurious signals: characterizing their properties, efficiency, and nature could ultimately lead to improved spatial resolution.
Finally, once the origins of these phenomena are better understood, machine-learning algorithms could be employed to address the complexity of SAT correction and to optimize the merging of timing information from different pads.

## 4 Conclusion

The studies reported here confirm the viability of the PICOSEC Micromegas concept as a scalable gaseous detector technology capable of providing time resolutions at the level of O(10) ps. Single-channel prototypes demonstrated that the choice and thickness of the photocathode play a crucial role in optimizing performance, with titanium and boron carbide ($B_4C$) emerging as promising alternatives to CsI thanks to their robustness and radiation hardness. Dedicated single-photoelectron studies highlighted the importance of advanced noise-rejection techniques to reliably extract amplitude distributions even when using fast amplifiers required for precision timing.
Regarding the multi-pad double-layer DLC prototype, the beam test analysis showed that spatial resolutions at the millimeter level can be achieved, although the intrinsic spread of Cherenkov photons imposes a fundamental limitation. Timing studies demonstrated that combining information from multiple pads either through a time-resolution-weighted approach or through a charge-weighted one provides comparable performances.
Overall, the results demonstrate that PICOSEC Micromegas detectors can achieve a good balance of excellent time resolution, scalability, robustness, and cost-effectiveness, establishing them as a strong candidate for future high-luminosity collider experiments. Further R&D efforts will focus on long-term stability studies, large-area integration, and advanced reconstruction techniques to fully exploit the potential of this technology.

## Acknowledgements

I would like to express my deepest gratitude to my supervisor, Marta, for giving me the chance to experience this unique journey at CERN, for guiding me through my first steps in the GDD laboratory and for always supporting me. Your passion for research, your remarkable expertise, the way you patiently taught me how to approach the work and your dedication to making GDD a friendly environment have meant so much to me personally and professionally.
I am also sincerely grateful to Eraldo and Florian for their readiness to engage in profound discussions on gaseous detectors and for their invaluable help during the analysis phase. Your expertise and commitment to the GDD projects have been a true source of inspiration and have strengthened my motivation to continue working in this field.
My thanks also go to the colleagues I had the pleasure to meet during the test beam weeks, in particular Antonija, Matteo and Thomas, whose support and insightful contributions helped me broaden my knowledge.
Finally, I would like to warmly thank the entire GDD family for making this experience truly unique, and especially all the other summer students with whom I had the privilege to share this stimulating and welcoming environment.

## References

[1] ECFA Detector R&D Roadmap Process Group. *The 2021 ECFA detector research and development roadmap.* Tech. rep. Geneva: CERN, 2020. DOI: 10.17181/CERN.XDPL.W2EX. URL: https://cds.cern.ch/record/2784893.

[2] Thomas Papaevangelou et al. *Fast Timing for High-Rate Environments with Micromegas.* 2016. arXiv: 1601.00123 [physics.ins-det]. URL: https://arxiv.org/abs/1601.00123.

[3] A. Utrobicic et al. *Single channel PICOSEC Micromegas detector with improved time resolution.* 2024. arXiv: 2406.05657 [physics.ins-det]. URL: https://arxiv.org/abs/2406.05657.

[4] Y. Giomataris et al. "MICROMEGAS: a high-granularity position-sensitive gaseous detector for high particle-flux environments". In: *Nuclear Instruments and Methods in Physics Research Section A: Accelerators, Spectrometers, Detectors and Associated Equipment* 376.1 (1996), pp. 29–35. ISSN: 0168-9002. DOI: https://doi.org/10.1016/0168-9002(96)00175-1. URL: https://www.sciencedirect.com/science/article/pii/0168900296001751.

[5] J. Bortfeldt et al. "PICOSEC: Charged particle timing at sub-25 picosecond precision with a Micromegas based detector". In: *Nuclear Instruments and Methods in Physics Research Section A: Accelerators, Spectrometers, Detectors and Associated Equipment* 903 (2018), pp. 317–325. ISSN: 0168-9002. DOI: https://doi.org/10.1016/j.nima.2018.04.033. URL: https://www.sciencedirect.com/science/article/pii/S0168900218305369.

[6] Ph. Abbon et al. "Micromegas, a microstrip detector for Compass". In: *Nuclear Instruments and Methods in Physics Research Section A: Accelerators, Spectrometers, Detectors and Associated Equipment* 461.1 (2001). 8th Pisa Meeting on Advanced Detectors, pp. 29–32. ISSN: 0168-9002. DOI: https://doi.org/10.1016/S0168-9002(00)01158-X. URL: https://www.sciencedirect.com/science/article/pii/S016890020001158X.

[7] David Attié et al. "Current Status and Future Developments of Micromegas Detectors for Physics and Applications". In: *Appl.Sciences* 11.12 (2021), p. 5362. DOI: 10.3390/app11125362. URL: https://hal.science/hal-03260794.

[8] J. Bortfeldt et al. "Modeling the timing characteristics of the PICOSEC Micromegas detector". In: *Nuclear Instruments and Methods in Physics Research Section A: Accelerators, Spectrometers, Detectors and Associated Equipment* 993 (2021), p. 165049. ISSN: 0168-9002. DOI: https://doi.org/10.1016/j.nima.2021.165049. URL: https://www.sciencedirect.com/science/article/pii/S0168900221000334.

[9] M. Lisowska et al. "Towards robust PICOSEC Micromegas precise timing detectors". In: *Journal of Instrumentation* 18.07 (July 2023), p. C07018. DOI: 10.1088/1748-0221/18/07/C07018. URL: https://dx.doi.org/10.1088/1748-0221/18/07/C07018.

[10] Marta Lisowska. "Exploring the potential of Micro-Pattern Gaseous Detectors technologies in High Energy Physics applications and beyond". Theses. Université Paris-Saclay, Sept. 2024. URL: https://theses.hal.science/tel-04867992.

[11] A. Utrobicic et al. "A large area 100-channel PICOSEC Micromegas detector with time resolution at the 20 ps level". In: *Journal of Instrumentation* 18.07 (July 2023), p. C07012. DOI: 10.1088/1748-0221/18/07/C07012. URL: https://dx.doi.org/10.1088/1748-0221/18/07/C07012.

[12] M. Lisowska et al. "Sub-25 ps timing measurements with 10 × 10 cm 2 PICOSEC Micromegas detectors". In: *Nuclear Instruments and Methods in Physics Research Section A Accelerators Spectrometers Detectors and Associated Equipment* 1046 (Jan. 2023), p. 167687. DOI: 10.1016/j.nima.2022.167687.

[13] C. Hoarau et al. "RF pulse amplifier for CVD-diamond particle detectors". In: *Journal of Instrumentation* 16.04 (Apr. 2021), T04005. ISSN: 1748-0221. DOI: 10.1088/1748-0221/16/04/t04005. URL: http://dx.doi.org/10.1088/1748-0221/16/04/T04005.

[14] D. Breton et al. "Measurements of timing resolution of ultra-fast silicon detectors with the SAMPIC waveform digitizer". In: *Nuclear Instruments and Methods in Physics Research Section A: Accelerators, Spectrometers, Detectors and Associated Equipment* 835 (2016), pp. 51–60. ISSN: 0168-9002. DOI: https://doi.org/10.1016/j.nima.2016.08.019. URL: https://www.sciencedirect.com/science/article/pii/S0168900216308373.

[15] Lukas Sohl. "Development of PICOSEC-Micromegas for fast timing in high rate environments". 2020UPASP084. PhD thesis. Université Paris-Saclay, 2020. URL: http://www.theses.fr/2020UPASP084/document.

[16] Neal Gallagher. "Savitzky-Golay Smoothing and Differentiation Filter". In: (Jan. 2020). DOI: 10.13140/RG.2.2.20339.50725.

[17] Chiara Volpato. *Photocathode studies for robust PICOSEC Micromegas detectors.* Tech. rep. Geneva: CERN, 2023. URL: https://repository.cern/records/gh16e-4h518.

[18] M.J. French et al. "Design and results from the APV25, a deep sub-micron CMOS front-end chip for the CMS tracker". In: *Nuclear Instruments and Methods in Physics Research Section A: Accelerators, Spectrometers, Detectors and Associated Equipment* 466.2 (2001). 4th Int. Symp. on Development and Application of Semiconductor Tracking Detectors, pp. 359–365. ISSN: 0168-9002. DOI: https://doi.org/10.1016/S0168-9002(01)00589-7. URL: https://www.sciencedirect.com/science/article/pii/S0168900201005897.

[19] S. Martoiu et al. "Development of the scalable readout system for micro-pattern gas detectors and other applications". In: *JINST* 8 (2013), p. C03015. DOI: 10.1088/1748-0221/8/03/C03015.

[20] M. Lisowska et al. "Photocathode characterisation for robust PICOSEC Micromegas precise-timing detectors". In: *Nuclear Instruments and Methods in Physics Research Section A: Accelerators, Spectrometers, Detectors and Associated Equipment* 1072 (2025), p. 170151. ISSN: 0168-9002. DOI: https://doi.org/10.1016/j.nima.2024.170151. URL: https://www.sciencedirect.com/science/article/pii/S0168900224010775.

[21] S. Aune et al. "Timing performance of a multi-pad PICOSEC-Micromegas detector prototype". In: *Nuclear Instruments and Methods in Physics Research Section A: Accelerators, Spectrometers, Detectors and Associated Equipment* 993 (2021), p. 165076. ISSN: 0168-9002. DOI: https://doi.org/10.1016/j.nima.2021.165076. URL: https://www.sciencedirect.com/science/article/pii/S0168900221000607.